THE JOURNAL OF PHYSICAL CHEMISTRY Letters

Letter

pubs.acs.org/JPCL

Direct Evidence of Confined Water in Room-Temperature Ionic Liquids by Complementary Use of Small-Angle X-ray and Neutron Scattering

Hiroshi Abe,*[,†] Takahiro Takekiyo,[‡] Machiko Shigemi,[‡] Yukihiro Yoshimura,[‡] Shu Tsuge,[§] Tomonori Hanasaki,[§] Kazuki Ohishi,[∥] Shinichi Takata,[⊥] and Jun-ichi Suzuki[∥]

[†]Department of Materials Science and Engineering and [‡]Department of Applied Chemistry, National Defense Academy, 1-10-20 Hashirimizu, Yokosuka 239-8686, Japan

[§]Department of Applied Chemistry, Ritsumeikan University, 1-1-1 Nojihigashi, Kusatsu, Shiga 525-8577, Japan

[∥]Research Center for Neutron Science and Technology, Comprehensive Research Organization for Science and Society (CROSS), IQBRC Bldg, 162-1 Shirakata, Tokai, Ibaraki 319-1106, Japan

[⊥]Japan Atomic Energy Agency, 2-4 Shirane Shirakata, Tokai, Ibaraki 319-1195, Japan

ABSTRACT: The direct evidence of confined water ("water pocket") inside hydrophilic room-temperature ionic liquids (RTILs) was obtained by complementary use of small-angle X-ray scattering and small-angle neutron scattering (SAXS and SANS). A large contrast in X-ray and neutron scattering cross-section of deuterons was used to distinguish the water pocket from the RTIL. In addition to nanoheterogeneity of pure RTILs, the water pocket formed in the water-rich region. Both water concentration and temperature dependence of the peaks in SANS profiles confirmed the existence of the hidden water pocket. The size of the water pocket was estimated to be ∼3 nm, and D_2O aggregations were well-simulated on the basis of the observed SANS data.

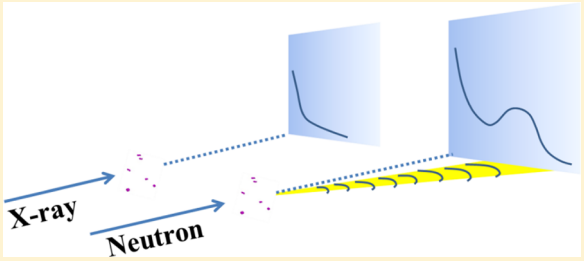

SECTION: Liquids; Chemical and Dynamical Processes in Solution

Room-temperature ionic liquids (RTILs) have been highlighted as novel solvents for green chemistry.[1−5] Their physicochemical properties depend on their inherent liquid structure. Structurally, their most fascinating feature is nanoheterogeneity, even when in a liquid state. In a pure RTIL system, size and distribution of nanoheterogeneity have been investigated experimentally[6−8] and theoretically.[9−14] In the typical imidazolium-based RTILs system (e.g., RTILs containing 1-alkyl-3-methylimidazolium cations; $C_n$mim$^+$), nanodomain size is proportional to the alkyl chain length, n.[7] Nanoheterogeneity is derived from polar and nonpolar components of RTILs.

Recently, mysterious hydrogen bonding of water in the RTILs has been reported. The effect of addition of water into [C_8mim][NO_3] was demonstrated by a molecular dynamics (MD) simulation.[15] At a concentration <80 mol % H_2O, bulk water is not formed in the simulation box. Water is confined near the nanodomain boundaries between the polar and nonpolar components. In another MD simulation,[16] [C_2mim]-[$EtSO_4$]−80 mol % H_2O reveals a critical mixing from chain-like water aggregation to the bicontinuous system, where $EtSO_4^-$ is ethylsulfate. Furthermore, an outstanding hierarchy structure is observed in the water-rich region of a hydrophilic RTIL−water system.[17,18] The RTIL was *N*,*N*-diethyl-*N*-methyl-*N*-(2-methoxyethyl)ammonium tetrafluoroborate, [DEME]-[BF_4], whose characteristics include a negative charge on the oxygen of the [DEME$^-$] cation[19] and numerous stable conformers[20] of the [DEME$^-$] cation. Hydrogen bonding can control the water-mediated network at short-range order, medium-range order (MRO), and long-range order. Both the liquid structure as well as macroscopic properties of [DEME]-[BF_4]−water mixtures exhibit anomalous optical absorption in the UV−vis region[21] as well as anomalous density and thermal properties,[22] AC impedance properties,[23] and pH values.[24,25]

Because of the mysterious hydrogen bonding of water in the RTILs, RTIL−water mixtures can possibly control protein structures. Very recently, we reported that lysozyme in [C_4mim][NO_3]−D_2O mixtures exhibits refolding, which is related to the confined water.[26] Dependence of lysozyme structure on water concentration was determined by small-angle X-ray scattering (SAXS). In contrast, β-lactoglobulin (β-LG), which has larger protein size than lysozyme, aggregates in [C_4mim][NO_3]−D_2O mixtures.[27] Aggregations of β-LG vary depending on water concentration and RTIL type. Confined water introduced into [C_4mim][NO_3] is key for elucidating intrinsic properties of the protein refolding and aggregation. We refer to this water as occupying a "water pocket". The water pocket corresponds to nonbulk water in the MD simulation.[15,16] However, as far as we know, direct evidence of the

Received: February 12, 2014
Accepted: March 10, 2014

   dx.doi.org/10.1021/jz500299z | *J. Phys. Chem. Lett.* 2014, 5, 1175−1180

water pocket in the RTILs has not been experimentally obtained. In principle, distinguishing the water pocket from the RTILs is difficult, primarily because scattering power of water is very small and the hydrogen of water is not sensitive to X-rays.

In this study, we experimentally extract the hidden water pocket using a complementary method that involves both SAXS and small-angle neutron scattering (SANS). The size and distribution of the water pocket are simulated using the SANS data.

Because of its neutron absorption and incoherent scattering abilities, the RTIL, $[C_4mim][NO_3]$ (Sigma-Aldrich), was used in this study. The water content in the as-received sample was 130−150 ppm, as determined from the Karl Fischer titration method. Using methods described in the literature,[28−31] we synthesized *N*,*N*-diethyl-*N*-methyl-*N*-(2-methoxyethyl)-ammonium nitrate, $[DEME][NO_3]$. Distilled D_2O (99.9%, Merck) was used as an additive. Because both RTILs are hydrophilic, the mixtures were prepared inside a glovebox under flowing helium gas.

SAXS experiments were conducted using a Kratky camera system (BioSAXS-1000, Rigaku) at a wavelength of 0.1542 nm. The incident beam was collimated using a parabolic multilayer mirror. Here the scattering vector q is defined as $4\pi(\sin\theta)/\lambda$ (nm^{-1}), where the scattered angle is 2θ. To eliminate air scattering, all assemblies were placed inside a vacuum chamber. Data were collected using a 2D detector (PILATUS 100K/R). Samples were placed in quartz capillaries with a diameter of 1.0 mm and a thickness of 0.1 mm. Time-of-flight SANS was performed on the BL15 (Taikan) instrument at the Japan Proton Accelerator Research Complex (J-PARC).[32] To simultaneously detect the scattering data from the wide q range, two kinds of area detectors were installed in the beamline. Data were collected from the small- and medium-angle detector banks in this study. A sample changer was mounted onto the goniometer. Temperature was controlled with a circulating bath (Ministat 125, Huber) The mixtures were placed into a quartz cell (Starna Scientific) with low neutron absorption ability. The thickness of the cells was 1.0 mm for $[DEME][NO_3]$ mixtures and 2.0 mm for $[C_4mim][NO_3]$ mixtures. The observed data were corrected with respect to the background, such as empty-cell and D_2O-filled-cell scattering. Using the multiple scattering model,[33] we estimated multiple scattering from the H of each cation in the simulation. By removing the long-wavelength components of incident neutron radiation, multiple scattering was almost suppressed. For example, with a restricted wavelength of 0.25 to 0.35 nm and $\Delta q/q$ = 0.12, scattering intensities in the small-angle detector bank were smoothly connected to those in the medium-angle bank. 2D data from both SAXS and SANS were reduced into 1D data because of isotropic scattering.

In the case of X-ray radiation, the scattering power of a deuteron is merely 3% that of a D_2O molecule. However, in the case of neutrons, the scattering power increases to 73% that of D_2O. With respect to extracting the positions of D_2O in the RTILs, this increased scattering in the complementary method provides a substantial advantage. SANS data were fitted by a model-dependent least-squares method via the program *SASfit*.[34] From the pair-distance distribution function obtained by *GNOM*,[35] ab initio modeling was performed using the *GASBOR*[31] program in the *ATSAS* software package[37−39] to determine the aggregation shape of the water pocket. The aggregation shape was approximately reconstructed with beads (i.e., with a dummy atom model) in the simulation box.

Comparison between Small-Angle X-ray Scattering and Neutron Scattering. The data-corrected SAXS patterns of $[C_4mim][NO_3]$−water mixtures at room temperature are shown in Figure 1. The red and blue circles in the Figure denote the

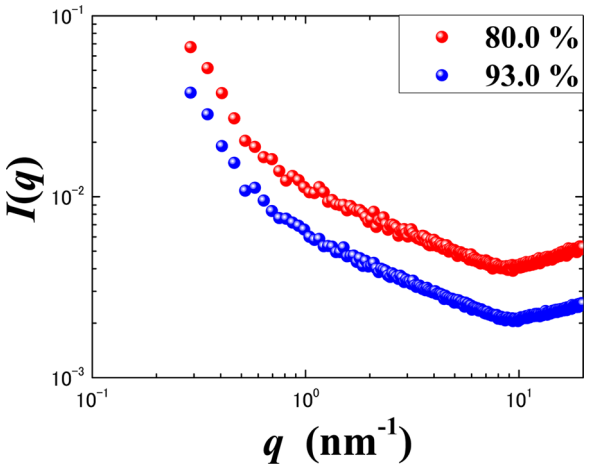

Figure 1. Small-angle X-ray scattering profiles of (a) $[C_4mim][NO_3]$−80.0 mol % D_2O (●, red) and (b) $[C_4mim][NO_3]$−93.0 mol % D_2O (●, blue) at room temperature.

$[C_4mim][NO_3]$−80.0 mol % and $[C_4mim][NO_3]$−93.0 mol % D_2O systems, respectively. The SAXS intensity of the sample with 80 mol % D_2O was greater than that of the sample with 93.0 mol % because of the large X-ray scattering power of the RTIL. No distinct peak was observed over the wide q range, unlike the case of pure RTILs.[7] Thus, RTILs' inherent nanoheterogeneity in the water-rich region of the $[C_4mim][NO_3]$−D_2O system was not detected by SAXS. We cannot probe the density fluctuations of the water pocket directly using only X-rays because of the lack of sensitivity of X-rays toward deuterated water.

In contrast, the SANS patterns at room temperature differed substantially from the SAXS pattern. The dependence of the SANS patterns on the water concentration in $[C_4mim][NO_3]$ and $[DEME][NO_3]$ is shown in Figures 2a,b, respectively. A significant finding is that a very weak but apparent peak appeared in the patterns of $[C_4mim][NO_3]$−D_2O mixtures with <95 mol % D_2O (Figure 2a). The concentration coincides with one of percolation limits estimated by the MD simulations.[16] At higher concentration, ionic liquid network peaks in the simulation box. Experimentally, density of $[DEME][BF_4]$−H_2O mixtures drastically changed at 90−95 mol %.[22] The experimentally obtained partial molar volumes of $[DEME][BF_4]$ and water were evaluated to be 202.2 and 17.9 (cm^3/mol), respectively. The average size was estimated to be 3 nm from the q position of the peak. The appearance of this peak in the SANS pattern, which was not observed in the SAXS pattern (Figure 1), confirms that the deuteron-contrasted water pocket is certainly detected via SANS. We stress that the complementary use of X-ray and neutron radiation is quite valid for less observable local fluctuations, such as those due to D_2O, compared with large scattering power of the RTILs. In addition, the trapezoid profile of the observed peak was not fitted by a simple Gaussian or Lorentzian function. Therefore, some intensity modulations were derived from the interference among the confined water. In contrast, the pattern of the $[DEME][NO_3]$−D_2O system included no peak in the

dx.doi.org/10.1021/jz500299z | *J. Phys. Chem. Lett.* 2014, 5, 1175−1180

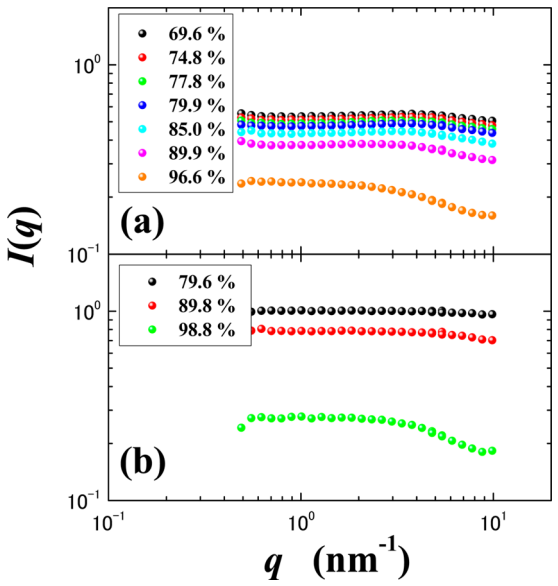

Figure 2. Small-angle neutron scattering (SANS) as a function of D_2O concentration of (a) $[C_4mim][NO_3]$- and (b) [DEME][NO_3]-based mixtures at room temperature. A distinct peak appeared in the SANS profile of the $[C_4mim][NO_3]$–D_2O system with a water content <90 mol %.

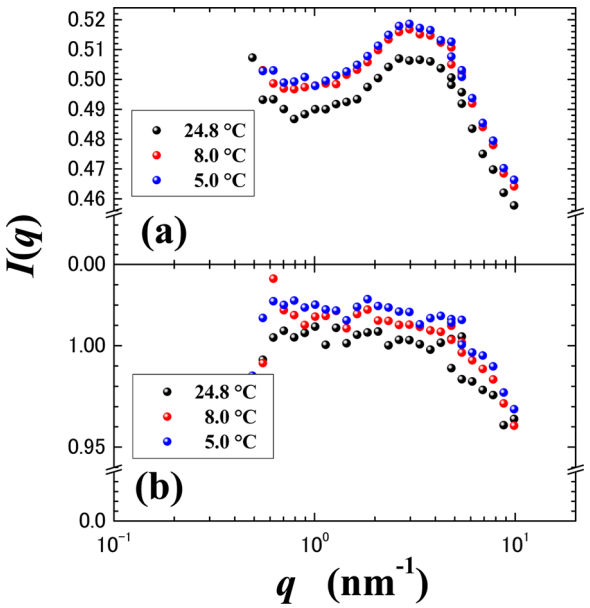

Figure 3. Temperature dependences of small-angle neutron scattering in (a) $[C_4mim][NO_3]$–77.8 mol % D_2O and (b) [DEME][NO_3]–79.6 mol % D_2O.

measured q region (Figure 2b). Hence, the water pocket observed in the $[C_4mim][NO_3]$–D_2O system is suppressed in the [DEME][NO_3]–D_2O system. Because the NO_3^- anion is common to both systems, the difference between C_4mim^+ and $DEME^+$ cation is key for interpreting the appearance/disappearance of the water pocket. With respect to the [DEME][NO_3]–D_2O system, one possible reason is that the oxygen of the $DEME^+$ cation acting as an electronegative component[19] disturbs the formation of the confined water. The oxygen of the cation might attract a deuteron of D_2O through hydrogen bonding as well as a NO_3^- anion. Among the nearly equivalent oxygen sites of both the cation and anion, the MRO of the water network develops without the formation of the water pocket. The network might be sustained by the dynamic motion of D_2O between two different oxygen sites. In the case of the $DEME^+$ cation system, we predict that a hierarchal structure is preferred to stabilize the liquid system under the hydrogen-bonding driven MRO network. In contrast, electronegative nitrogen of C_4mim^+ cation might not capture a deuteron of D_2O. This is because nitrogen is bonded to hydrophobic methyl or butyl chain and has little space geometrically. The motion of hydrophobic tail groups of cation might weaken hydrogen bonding between hydrophilic head groups of cation and a deuteron of D_2O. Also, the MD simulations of $[C_4mim][BF_4]$–H_2O support the weak interaction between cation and water.[40] The interaction is suppressed by the size and anisotropy of cation.

Thermal Properties of Confined Water. To investigate the thermal stability of the water pocket, we measured the temperature dependence of the SANS patterns of $[C_4mim][NO_3]$–77.8 mol % D_2O and [DEME][NO_3]–79.6 mol % D_2O (Figure 3a,b). The logarithmic scale of the SANS intensity was converted to a linear scale to emphasize the SANS peak profile. In the linear plot, the SANS of the [DEME][NO_3]–79.6 mol % D_2O was slightly modulated, although no distinct peak was observed (Figure 3b). Here the experimental conditions in [DEME][NO_3]–79.6 mol % D_2O are a measurement time of 2 h and a cell thickness of 1 mm. At lower temperatures, no peak in the SANS pattern was observed, and the SANS intensity increased slightly. Hence the water pocket did not form in the [DEME][NO_3]–79.6 mol % D_2O mixture at low temperatures. The MRO of the water network did not collapse even at low temperatures. In contrast, in the case of $[C_4mim][NO_3]$–77.8 mol % D_2O (measurements time of 2 h and cell thickness of 2 mm), a trapezoidal peak was observed in the SANS patterns as a function of temperature, which indicates a thermal effect of the water pocket. Obviously, the SANS intensities increased at low temperatures; however, the total scattering is explained merely by an increase in the baseline without any peak shifts or sharpening/broadening. This result indicates that the size and distribution of the water pocket are invariant from 24.8 to 5.0 °C; however, different types of local fluctuations are induced at low temperatures. The thermally invariant confined water is realized because of the rigid confinement of theoretically predicted nanodomain boundaries.[15]

SANS Analysis and Modeling of Local Fluctuations. Theoretical approaches are indispensable in resolving the complicated heterogeneity in the liquids. To acquire reliable statistics, we performed 8 h measurements on the $[C_4mim][NO_3]$–77.8 mol % D_2O system at 5 °C. We first fitted the observed data using the model-dependent *SASfit* program,[34] which is a least-squares fitting program that incorporates numerous models. Among the available models, the Teubner–Strey phenomenological model (TS model)[41,42] is the most adequate for modeling the water pocket because other models in *SASfit* cannot adequately reproduce the observed peak. The profile fitted using the TS model and a Maxwell size distribution for $[C_4mim][NO_3]$–77.8 mol % D_2O at 5 °C is shown by the green curve in Figure 4a. The TS model was originally developed on the basis of the Landau theory to explain microemulsions consisting of a binary oil–water system. We suppose that the formation of the weakly formed ambiguous boundaries of the microemulsions is very similar to that of the water pocket, whose boundary is ambiguous in the MD simulation.[15,16] However, the TS model

dx.doi.org/10.1021/jz500299z | J. Phys. Chem. Lett. 2014, 5, 1175–1180

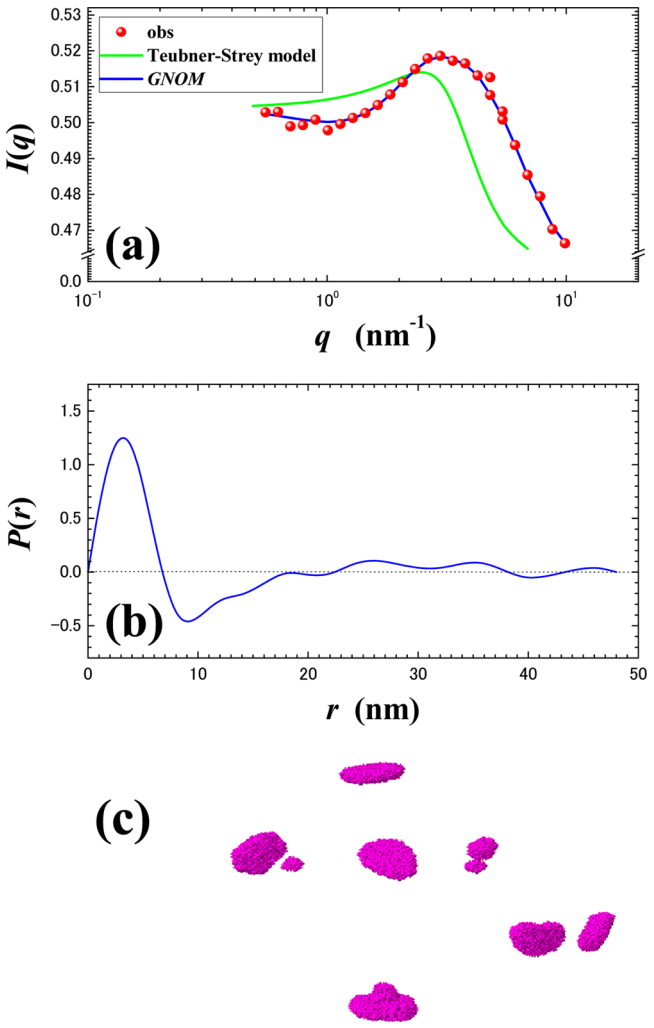

Figure 4. (a) Small-angle neutron scattering intensities, $I(q)$, of $[C_4mim][NO_3]$−77.8 mol % D_2O at 5 °C and (b) pair-distance distribution functions, $P(r)$, and (c) ab initio simulation results based on $I(q)$ and $P(r)$. The green curve in panel a is obtained by the Teubner−Strey phenomenological model. Blue curves in panel a reveal $I(q)$ optimized by indirect Fourier transformation.

is still not sufficient to extrapolate the trapezoidal peak profile. In recent SANS analyses,[39] further progress has been made in the analysis of the local structures in noncrystalline materials. The *ATSAS* software package[37−39] is commonly used in model-free simulations. First, the pair-distance distribution function $P(r)$ was calculated using the indirect Fourier transformation (FT) program *GNOM*.[35] $P(r)$ was determined through the optimization of parameters to fit the observed data, $I(q)$. In the case of $[C_4mim][NO_3]$−77.8 mol % D_2O at 5 °C, the calculated $P(r)$ in Figure 4b simultaneously provides the optimized $I(q)$ in reciprocal space, which is indicated by the blue curve in Figure 4a. In comparison with the conventional TS model, the indirect FT approach can reproduce the observed data almost perfectly. The other determinant of calculation accuracy is the convergence of $P(r)$ at $r \to 0$ and $r \to r_{max}$. With both of these conditions satisfied (i.e., a well-fitted $I(q)$ and the convergence of $P(r)$), we successfully analyzed the complicated SANS profile. We subsequently observed that $P(r)$ revealed additional medium range oscillations. The oscillation of $P(r)$ over the medium-range indicates that some interference between the water pocket is not ignored. For simplicity, the total scattering I^{total} is expressed by

$$I^{total} = I^{RTIL} + I^{D_2O} + I^{RTIL} * I^{D_2O} \quad (1)$$

where * indicates convolution as a coupling term between the RTIL contribution (I^{RTIL}) and D_2O contribution (I^{D_2O}). The third term in eq 1 is influenced by the correlation between the RTIL nanoheterogeneity and the water pocket on the basis of diffraction theory. The trapezoidal profile indicates that the water pocket interacts with other pockets through the RTIL media.

Ab Initio Simulation to Visualize the Water Pocket. In the case of complicated systems, graphical representations by computer-aid simulations enable us to directly recognize anisotropic shapes and arrangements of aggregations in real space. Although the simulation results are merely one ensemble in real time and space, the results become a fingerprint to address primary/secondary structures. The ab initio bead modeling of one component enables the visualization of complicated local fluctuations, such as protein solutions, with 15% errors.[39] In this study, one component of D_2O was approximately simulated in a $[C_4mim][NO_3]$−D_2O system, because only D_2O exhibits enhanced SANS. Hence, the nonenhancement term I^{RTIL} in eq 1 was not considered in the calculations. *GASBOR*[36] is a promising ab initio modeling program that uses monodisperse beads (i.e., dummy-atom models). We selected the refinement using $P(r)$ in real space because the simulation of the observed $I(q)$ in reciprocal space provided poor reproduction of $I(q)$. $P(r)$ modulated over the medium-range is a good constraint to express the water pocket. The optimized shape and distribution of the water pocket were reconstructed, as shown in Figure 4c. Aggregations of a comparable size are located with a specific distance among them. In the $[C_4mim][NO_3]$−D_2O system, the water pocket visualized on the basis of SANS data is similar to the confined water in the MD simulation of the $[C_8mim][NO_3]$−H_2O[15] and $[C_2mim][EtSO_4]$−H_2O.[16]

In this study, theoretically predicted confined water is experimentally verified for the first time by the complementary use of X-ray and neutron radiation. In the $[C_4mim][NO_3]$−D_2O system, the D_2O concentration and temperature dependence of the distinct peak in the SANS profile provide direct proof of the water pocket inside the RTILs. The size of the water pocket is ∼3 nm. However, indirect FT methods and refinements of the observed $I(q)$ can estimate the pair-distance distribution function $P(r)$. The ab initio modeling of neutron-enhanced D_2O on the basis of $P(r)$ approximately demonstrates the size, shape, and distribution of the water pocket on the mesoscopic scale. This result of the present study will help in clarifying the mechanism of the hierarchy,[18] the existence of nearly free hydrogen bonds even at 77 K[43] in the $[DEME][BF_4]$−water system, and protein refolding in $[C_4mim][NO_3]$−D_2O mixtures.[26] Mysterious water behavior in the water-rich region might be due to simple balancing among the charge (scalar), orientational order (vector), and coordination number (topology).[44]

AUTHOR INFORMATION

Corresponding Author

*E-mail: ab@nda.ac.jp.

Notes

The authors declare no competing financial interest.

■ ACKNOWLEDGMENTS

We thank Dr. T. Matsumoto of Rigaku Co. for experimental support and helpful discussions. We also thank Dr. M. Aono of the National Defense Academy and Professor A. Shimizu of Soka University for helpful discussions. We acknowledge the support of J-PARC; activity under "Hierarchy Structure in Hydrogen Bonding Assisted System: Room Temperature Ionic Liquid-Water Mixture" program (Proposal No. 2012B0001).

■ REFERENCES

(1) Blanchard, L. A.; Hâncu, D.; Beckman, E. J.; Brennecke, J. F. Green Processing Using Ionic Liquids and CO_2. *Nature* **1999**, *399*, 28−29.
(2) Leitner, W. A Greener Solution. *Nature* **2003**, *423*, 930−931.
(3) Earle, M. J.; Esperanca, J. M. S. S.; Gilea, M. A.; Lopes, J. N. C.; Rebelo, L. P. N.; Magee, J. W.; Seddon, K. R.; et al. The Distillation and Volatility of Ionic Liquids. *Nature* **2006**, *439*, 831−834.
(4) Brennecke, J. F.; Gurkan, B. E. Ionic Liquids for CO_2 Capture and Emission Reduction. *J. Phys. Chem. Lett.* **2010**, *1*, 3459−3464.
(5) Tang, J.; Tang, H.; Sun, W.; Plancher, H.; Radosza, M.; Shen, Y. Poly(ionic liquid)s: a New Material with Enhanced and Fast CO_2 Absorption. *Chem. Commun.* **2005**, 3325−3327.
(6) Triolo, A.; Russina, O.; Bleif, H-. J.; Cola, E. D. Nanoscale Segregation in Room Temperature Ionic Liquids. *J. Phys. Chem. B* **2007**, *111*, 4641−4644.
(7) Russina, O.; Triolo, A.; Gontrani, L.; Caminiti, R.; Xiao, D.; Hines, L. G., Jr.; Bartsch, R. A.; et al. Morphology and Intermolecular Dynamics of 1-Alkyl-3-methylimidazolium Bis{(trifluoromethane)-sulfonyl}amide Ionic Liquids: Structural and Dynamic Evidence of Nanoscale Segregation. *J. Phys.: Condens. Matter* **2009**, *21*, 424121-1−424121-9.
(8) Annapureddy, H. V. R.; Kashyap, H. K.; De Biase, P. M.; Margulis, C. J. What Is the Origin of the Prepeak in the X-ray Scattering of Imidazolium-Based Room-Temperature Ionic Liquids? *J. Phys. Chem. B* **2010**, *114*, 16838−16846.
(9) Urahata, S. M.; Ribeiro, M. C. C. Structure of Ionic Liquids of 1-Alkyl-3-methylimidazolium Cations: A Systematic Computer Simulation Study. *J. Chem. Phys.* **2004**, *120*, 1855−1863.
(10) Wang, Y.; Voth, G. A. Unique Spatial Heterogeneity in Ionic Liquids. *J. Am. Chem. Soc.* **2005**, *127*, 12192−12193.
(11) Canongia Lopes, J. N. A.; Pádua, A. A. H. Nanostructural Organization in Ionic Liquids. *J. Phys. Chem. B* **2006**, *110*, 3330−3335.
(12) Wang, Y.; Voth, G. A. Tail Aggregation and Domain Diffusion in Ionic Liquids. *J. Phys. Chem. B* **2006**, *110*, 18601−18608.
(13) Habasaki, J.; Ngai, K. L. Heterogeneous Dynamics of Ionic Liquids from Molecular Dynamics Simulations. *J. Chem. Phys.* **2008**, *129*, 194501-1−194501-15.
(14) Shimizu, K.; Pádua, A. A. H.; Lopes, J. N. C. Nanostructure of Trialkylmethylammonium Bistriflamide Ionic Liquids Studied by Molecular Dynamics. *J. Phys. Chem. B* **2010**, *114*, 15635−15641.
(15) Jiang, W.; Wang, Y.; Voth, G. A. Molecular Dynamics Simulation of Nanostructural Organization in Ionic Liquid/Water Mixtures. *J. Phys. Chem. B* **2007**, *111*, 4812−4818.
(16) Bernardes, C. E. S.; Minas da Piedade, M. E.; Canongia Lopes, J. N. The Structure of Aqueous Solutions of a Hydrophilic Ionic Liquid: The Full Concentration Range of 1-Ethyl-3-methylimidazolium Ethylsulfate and Water. *J. Phys. Chem. B* **2011**, *115*, 2067−2074.
(17) Aono, M.; Imai, Y.; Ogata, Y.; Abe, H.; Goto, T.; Yoshimura, Y.; Takekiyo, T.; et al. Anomalous Mixing State in Room-Temperature Ionic Liquid-Water Mixtures: *N,N*-Diethyl-*N*-methyl-*N*-(2-methoxyethyl) Ammonium Tetrafluoroborate. *Metall. Mater. Trans.* **2011**, *42A*, 37−40.
(18) Abe, H.; Yoshimura, Y. *Ionic Liquids: Theory, Properties, New Approaches*; Intech Publishing: Rijeka, Croatia, 2011.
(19) Tsuzuki, S.; Hayamizu, K.; Seki, S.; Ohno, Y.; Kobayashi, Y.; Miyashiro, H. Quaternary Ammonium Room-Temperature Ionic Liquid Including an Oxygen Atom in Side Chain/Lithium Salt Binary Electrolytes: Ab Initio Molecular Orbital Calculations of Interactions between Ions. *J. Phys. Chem. B* **2008**, *112*, 9914−9920.
(20) Takekiyo, T.; Imai, Y.; Abe, H.; Yoshimura, Y. Conformational Analysis of Quaternary Ammonium-Type Ionic Liquid Cation, *N,N*-diethyl-*N*-methyl-*N*-(2-methoxyethyl) Ammonium Cation. *Adv. Phys. Chem* **2012**, 829523-1−829523-7.
(21) Aono, M.; Imai, Y.; Abe, H.; Matsumoto, H.; Yoshimura, Y. UV−vis Spectroscopic Study of Room Temperature Ionic Liquid−Water Mixtures: *N,N*-Diethyl-*N*-methyl-*N*-(2-methoxyethyl) Ammonium Tetrafluoroborate. *Thermochim. Acta* **2012**, *532*, 179−182.
(22) Abe, H.; Mori, T.; Imai, Y.; Yoshimura, Y. Water Desorption Process in Room Temperature Ionic Liquid-H_2O Mixtures: *N,N*-Diethyl-*N*-methyl-*N*-(2-methoxyethyl) Ammonium Tetrafluoroborate. *J. Thermodyn.* **2012**, 351968-1−351968-5.
(23) Abe, H.; Aono, M.; Yoshimura, Y. Impedance Spectroscopic Study on Room Temperature Ionic Liquid-Water Mixtures. *J. Chem. Chem. Eng.* **2012**, *6*, 383−390.
(24) Aono, M.; Tomita, Y.; Abe, H.; Yoshimura, Y. Nonequilibrium Acidic Fluctuations in Room-Temperature Ionic Liquid/Water Mixture: *N,N*-diethyl-*N*-methyl-*N*-(2-methoxyethyl)ammonium Tetrafluoroborate. *Chem. Lett.* **2012**, *41*, 1532−1534.
(25) Aono, M.; Abe, H.; Takekiyo, T.; Yoshimura, Y. Protonated/Deprotonated Properties of a Room Temperature Ionic Liquid-Water System: *N,N*-Diethyl-*N*-methyl-*N*-2-methoxyethyl Ammonium Tetrafluoroborate. *Chem. Phys. Lett.*, in press.
(26) Takekiyo, T.; Yamazaki, K.; Yamaguchi, E.; Abe, H.; Yoshimura, Y. High Ionic Liquid Concentration-Induced Structural Change of Protein in Aqueous Solution: A Case Study of Lysozyme. *J. Phys. Chem. B* **2012**, *116*, 11092−11097.
(27) Takekiyo, T.; Koyama, Y.; Yamazaki, K.; Abe, Y.; Yoshimura, Y. Ionic Liquid-Induced Formation of the α-Helical Structure of β-Lactoglobulin. *J. Phys. Chem. B* **2013**, *117*, 10142−10148.
(28) Sato, T.; Masuda, G.; Takagi, K. Electrochemical Properties of Novel Ionic Liquids for Electric Double Layer Capacitor Applications. *Electrochim. Acta* **2004**, *49*, 3603−3611.
(29) Zhou, Z. B.; Matsumoto, H.; Tatsumi, K. Low-Melting, Low-Viscous, Hydrophobic Ionic Liquids: Aliphatic Quaternary Ammonium Salts with Perfluoroalkyltrifluoroborates. *Chem.—Eur. J.* **2005**, *11*, 752−766.
(30) Imai, Y.; Abe, H.; Matsumoto, H.; Shimada, O.; Hanasaki, T.; Yoshimura, Y. Glass Transition Behaviour of the Quaternary Ammonium Type Ionic Liquid, {[DEME][I] + H_2O} Mixtures. *J. Chem. Thermodyn.* **2011**, *43*, 319−322.
(31) Yoshimura, Y.; Hatano, N.; Imai, Y.; Abe, H.; Shimada, O.; Hanasaki, T. Glass Transition Behavior of the Quaternary Ammonium-Type Ionic Liquid: *N,N*-Diethyl-*N*-methyl-*N*-(2-methoxyethyl)ammonium Bromide-H_2O Mixtures. *J. Thermodyn.* **2012**, 575728-1−575728-6.
(32) Shinohara, T.; Takata, S.; Suzuki, J.; Oku, T.; Suzuya, K.; Aizawa, K.; Arai, M.; et al. Design and Performance Analyses of the New Time-of-Flight Smaller-Angle Neutron Scattering Instrument at J-PARC. *Nucl. Instrum. Methods Phys. Res., Sect. A* **2009**, *600*, 111−113.
(33) Shibayama, M.; Nagao, M.; Okabe, S.; Karino, T. Evaluation of Incoherent Neutron Scattering from Softmatter. *J. Phys. Soc. Jpn.* **2005**, *74*, 2728−2736.
(34) Kohlbrecher, J. *SASfit*; Berlin Neutron Scattering Centre (BENSC): Berlin, 2000.
(35) Svergun, D. I. Determination of the Regularization Parameter in Indirect-Transform Methods Using Perceptual Criteria. *J. Appl. Crystallogr.* **1992**, *25*, 495−503.
(36) Svergun, D. I.; Petoukhov, M. V.; Koch, M. H. Determination of Domain Structure of Proteins from X-ray Solution Scattering. *Biophys. J.* **2001**, *80*, 2946−2953.
(37) Konarev, P. V.; Petoukhov, M. V.; Volkov, V. V.; Svergun, D. I. ATSAS 2.1, A Program Package for Small-Angle Scattering Data Analysis. *J. Appl. Crystallogr.* **2006**, *39*, 277−286.
(38) Petoukhov, M. V.; Konarev, P. V.; Kikhney, A. G.; Svergun, D. I. ATSAS 2.1 - Towards Automated and Web-Supported Small-Angle Scattering Data Analysis. *J. Appl. Crystallogr.* **2007**, *40*, s223−s228.

(39) Petoukhov, M. V.; Franke, D.; Shkumatov, A. V.; Tria, G.; Kikhney, A. G.; Gajda, M.; Gorba, C.; et al. New Developments in the ATSAS Program Package for Small-Angle Scattering Data Analysis. *J. Appl. Crystallogr.* **2012**, *45*, 342−350.
(40) Schröder, C.; Rudas, T.; Neumayr, G.; Benkner, S.; Steinhauser, O. On the Collective Network of Ionic Liquid/Water Mixtures. I. Orientational Structure. *J. Chem. Phys.* **2007**, *127*, 234503.
(41) Teubner, M.; Strey, R. Origin of the Scattering Peak in Microemulsions. *J. Chem. Phys.* **1987**, *87*, 3195−3200.
(42) Schubert, K. −V.; Strey, R.; Kline, S. R.; Kaler, E. W. Small Angle Neutron Scattering near Lifshitz Lines: Transition from Weakly Structured Mixtures to Microemulsions. *J. Chem. Phys.* **1994**, *101*, 5343−5355.
(43) Yoshimura, Y.; Goto, T.; Abe, H.; Imai, Y. Existence of Nearly-Free Hydrogen Bonds in an Ionic Liquid, *N*,*N*-Diethyl-*N*-methyl-*N*-(2-methoxyethyl) Ammonium Tetrafluoroborate-Water at 77 K. *J. Phys. Chem. B* **2009**, *113*, 8091−8095.
(44) Abe, H.; Takekiyo, T.; Hatano, N.; Shigemi, M.; Hamaya, N.; Yoshimura, Y. Pressure-Induced Frustration−Frustration Process in 1-Butyl-3-methylimidazolium Hexafluorophosphate, A Room-Temperature Ionic Liquid. *J. Phys. Chem. B* **2014**, *118*, 1138−1145.